



HAL
open science

Heat transfer modification of a natural convection flow in a differentially heated cavity by means of a localized obstacle

P. Chorin, Florian Moreau, D. Saury

► **To cite this version:**

P. Chorin, Florian Moreau, D. Saury. Heat transfer modification of a natural convection flow in a differentially heated cavity by means of a localized obstacle. *International Journal of Thermal Sciences*, 2020, 151, pp.106279. 10.1016/j.ijthermalsci.2020.106279 . hal-02467416

HAL Id: hal-02467416

<https://hal.science/hal-02467416>

Submitted on 21 Jul 2022

HAL is a multi-disciplinary open access archive for the deposit and dissemination of scientific research documents, whether they are published or not. The documents may come from teaching and research institutions in France or abroad, or from public or private research centers.

L'archive ouverte pluridisciplinaire **HAL**, est destinée au dépôt et à la diffusion de documents scientifiques de niveau recherche, publiés ou non, émanant des établissements d'enseignement et de recherche français ou étrangers, des laboratoires publics ou privés.



Distributed under a Creative Commons Attribution - NonCommercial 4.0 International License

Heat transfer modification of a natural convection flow in a differentially heated cavity by means of a localized obstacle

P. Chorin, F. Moreau, D. Saury

Institut Pprime, UPR CNRS 3346, ISAE-ENSMA - CNRS - Université de Poitiers, BP 40109 - 86961 Chasseneuil Futuroscope, France

Abstract

In this experimental study, a natural convection flow in a differentially heated cavity has been disturbed in order to modify heat transfers. The disturbance is achieved by introducing a localized obstacle which acts as a small spatial extent passive system. The obstacle is placed inside the hot boundary layer of the cavity flow. Measurements have been carried out in terms of velocity fields, temperature profiles and heat transfers. The influence of the length and the vertical location for an insulating and a conducting obstacle have been analyzed. For the insulating obstacle, a part of the flow is deviated inside the colder core region in front of the obstacle, which leads to an increase of the downstream heat transfers as the deviated colder flow returns along the hot wall. For the conducting obstacle, a hot thermal plume is generated, which counters the obstacle effect observed for the insulating obstacle. In that case, the downstream heat transfer is increased or reduced depending on the vertical location of the obstacle. Relative changes on heat transfers compared to the case without obstacle are larger for longer obstacles and for higher vertical locations of the obstacle, for any conductivity. For instance, a relative heat transfer increase up to 83% is observed downstream the insulating obstacle for the largest length and highest vertical location.

Keywords: Natural convection, Differentially heated cavity, Heat transfer modification.

Email addresses: florian.moreau@ensma.fr (F. Moreau), didier.saury@ensma.fr (D. Saury)

Preprint submitted to International Journal of Thermal Sciences

13 janvier 2020

Nomenclature

A	aspect ratio
D	cavity depth, m
g	gravitational acceleration, $m.s^{-2}$
H	cavity height (reference length), m
l	dimensionless cylindrical obstacle length (scaled by H)
L	cavity width, m
$Nu_{1D}(Z)$	local Nusselt number, $Nu_{1D}(Z) = -\frac{\partial\theta}{\partial X}(Y = 0.146, Z)$
Pr	Prandtl number, $Pr = \nu/\alpha$
r	dimensionless cylindrical obstacle radius (scaled by H)
Ra_H	Rayleigh number based on cavity height, $Ra_H = \frac{g\beta\Delta TH^3}{\nu\alpha}$
S	stratification parameter, $S = \frac{\partial\theta}{\partial Z}(X = 0.125, Y = 0.146, Z = 0.50)$
t	dimensionless time (scaled by $H^2/(\alpha\sqrt{Ra_H})$)
T	temperature, K
T_0	mean temperature in the cavity, $T_0 = \frac{1}{2}(T_h + T_c)$, K
U, V, W	dimensionless velocities (scaled by $\alpha\sqrt{Ra_H}/H$)
x, y, z	physical cartesian coordinates, m
X, Y, Z	dimensionless coordinates, $(X, Y, Z) = (x, y, z)/H$

Greek symbols

α	thermal diffusivity, $m^2.s^{-1}$
β	thermal expansion coefficient, K^{-1}
ΔT	temperature difference between the isothermal walls, $\Delta T = T_h - T_c$, K
δ	dynamic boundary layer thickness
ε	wall emissivity
λ	thermal conductivity, $W.m^{-1}.K^{-1}$
ν	cinematic viscosity, $m^2.s^{-1}$
ρ	density, $kg.m^{-3}$
θ	dimensionless temperature, $\theta = (T - T_0)/\Delta T$

Subscripts and superscripts

c	cold
d	downstream
h	hot
hori	horizontal
rel	relative to the cylindrical obstacle
ref	reference value
u	upstream
vert	vertical

Abbreviations

CO	Cylindrical Obstacle
DHC	Differentially Heated Cavity
RB	Rayleigh-Benard

1. Introduction

Natural convection occurs in nature in many meteorological and geophysical situations as well as in many industrial applications. Close cavities are good candidates to study natural convection since boundary conditions are well defined which is crucial to understand the underlying physics or for further numerical simulations. Natural convection in enclosed parallelepipedic cavities usually appears into two configurations : the Rayleigh-Benard (RB) configuration and the Differentially Heated Cavity (DHC) configuration, for which the isothermal walls are respectively orthogonal and parallel to the direction of gravity. In this work, the DHC has been considered. This configuration is encountered in a wide range of applications such as cooling processes for electronic devices, solar collectors, nuclear power plants, in the under-hood space of cars or in building design for thermal comfort. In this configuration, due to the temperature difference between the vertical isothermal walls, a movement of the fluid arises. When this difference increases, the flow turns into a vertical boundary layer flow with jets along the horizontal walls, whereas the central zone remains almost at rest and stratified in temperature. In the past decades, differentially heated cavities have been widely studied theoretically, experimentally and numerically from laminar to transient and turbulent flows [1, 2, 3, 4, 5, 6].

Heat transfer enhancement has been studied in this configuration through several strategies. Indeed, the flow developing in a DHC can be disturbed within the objective of acting on heat transfers of the isothermal walls. Several studies have shown that the flow can be actively modified by mechanical [7],

acoustic [8] or thermal [9, 10] disturbances or cavity inclination [11]. These modifications by active systems require a continuous external action and induce an additional energy consumption and maintenance. Another solution is the use of a passive disturbance.

One way to act on a natural convection flow passively is to introduce wall roughness, the walls being normally considered as smooth walls. Several shapes and sizes of roughnesses have been previously studied both in RB and DHC configurations. In the RB configuration, Du and Tong [12] studied experimentally the influence of pyramidal grooves on the isothermal walls. For $10^9 \leq Ra \leq 10^{11}$, the authors observed an increase of 76% of heat transfer compared to the smooth wall case. Salort et al. [13] placed square-studs on the hot bottom wall. They observed that on the rough wall the overall Nusselt number is larger due to a local increase in transfers above the studs, which is greater than their reduction in the notches. In the DHC configuration, Yousaf and Usman [14] placed sinusoidal roughness elements on the vertical walls of a square cavity. At $Ra = 10^6$ and for 10 roughness elements, the authors observed a reduction in the overall Nusselt number up to 17%.

Another passive disturbance in the DHC configuration is the insertion of one or more fins positioned on the walls. These fins are either insulating or highly conducting, and a variety of sizes and locations have been studied. One of the first studies with this kind of perturbation disturbance was done by Shakerin et al. [15]. For a conducting fin placed on the hot wall of a square cavity, the calculation of the global heat transfer indicated an increase of the Nusselt number of 12%. This increase is limited by the deviation of the flow and the resulting thickening of the boundary layer upstream and downstream the fin. Nag et al. [16] studied numerically the influence of an infinitesimal-thick fin on the hot wall for several lengths and locations. The authors showed that the Nusselt number on the cold side increases with a perfectly conducting fin and decreases with an adiabatic one. Polidori and Padet [17] positioned three adiabatic fins on a vertical plate heated with a uniform heat flux and immersed in a water tank. The authors noted a circulation of the fluid in the area between the fins, an increase of the convective exchange coefficient close to the lower fin and a reduction close to the upper one. Tasnim and Collins [18] studied numerically, in a square cavity, the influence of a thin and perfectly conducting fin for Rayleigh numbers up to 10^5 . An increase of overall heat transfers is observed, especially when the fin length is large (up to 31% for the largest size). In several experimental and numerical studies, Xu et al. [19, 20] and Xu [21] positioned an adiabatic fin at the mid-height of a DHC with a vertical shape ratio equal to 0.24 and filled with water. The authors showed that above a certain Rayleigh number, the fin creates an unsteady flow by the periodic formation of thermal plumes. Therefore,

with a fin on each active wall, the Nusselt number increases by 7%. Recently, Ghalambaz et al. [22] used a flexible fin at mid-height with a sinusoidal oscillation imposed at the end of the fin. At $Ra = 10^6$, the authors showed that, compared to a static fin, the overall Nusselt number increases slightly with amplitude and period. In addition, the gain is more important when the fin is more flexible. To sum up, in absence of a change in the flow regime, adding a fin leads to an increase in global heat transfers if the fin is conducting and to a decrease if the fin is insulating.

A last category of passive disturbance of a natural convection flow in a confined enclosure is the use of discrete elements or obstacles. Unlike fins, they are not necessarily located on the walls and can have a large size. Merrikh and Lage [23] placed several solid blocks within a square cavity. They showed that the deviation of the flow into the inner core of the cavity reduces drastically the wall heat transfers. Laguerre et al. [24] positioned in a rectangular cavity an arrangement of 40 cylindrical obstacles parallel to the cold wall. These obstacles are 10 times smaller in size than the width of the cavity. The fluid is humid air and the flow is described in terms of temperature, flow velocity and moisture. They observed a modification of the cold boundary layer flow due to the presence of obstacles, which induces a flow circulation in the areas between them.

These studies demonstrate the possibility to act on natural convection flows by means of fins and obstacles, in order to modify heat transfers. These disturbances occupy generally a large space within the cavity. In order to reduce the size and therefore the mass and the cost of such devices, a localized disturbance is used in this experimental study. The disturbance is a cylindrical obstacle of small spatial extent, with a maximal length equal to 4% of the height of the cavity. The obstacle is placed on the hot wall of the cavity.

The purpose of this work is to study the modification of heat transfers downstream an obstacle. We will first introduce the DHC experimental set-up and the measurement methods that have been used to investigate the flow and the associated heat transfers. Then the results concerning the disturbed flow (especially in terms of velocity fields and temperature profiles) and the associated heat transfers are analyzed and compared to those of the undisturbed flow.

2. Experimental set-up

2.1. DHC description

The Differentially Heated Cavity (DHC) used in this study is a parallelepiped with the following internal dimensions : width $L = 12$ cm, depth

$D = 14$ cm, height $H = 48$ cm (see Fig. 1). Those three dimensions are respectively associated with the x, y and z axes. The vertical and horizontal aspect ratios are equal to $A_{vert} = \frac{H}{L} = 4$ and $A_{hori} = \frac{D}{L} = 1.167$.

The vertical walls, with an imposed temperature, are made of duralumin (conductivity $\lambda = 164 \text{ W.m}^{-1}.\text{K}^{-1}$, emissivity $\varepsilon \in [0.1; 0.2]$) with a thickness of 5 mm. A vertical slit of 10 mm width is located at the mid-depth of the cold wall to let a laser sheet pass through a glass window for PIV measurements. It has been checked that the slit has no influence on the dynamics of the flow. Thus, due to this experimental limitation, all the measurements presented in this work were carried out along the vertical mid-depth plane.

The horizontal walls are made of expanded polystyrene with very low conductivity ($\lambda = 0.035 \text{ W.m}^{-1}.\text{K}^{-1}$, 9 cm in thick for the bottom wall and 16 cm in thick for the top wall) and covered with an aluminum foil to minimize radiative exchanges ($\varepsilon = 0.080 \pm 0.005$).

The measurement cavity is framed by two guard cavities with the same dimensions and located behind and in front of it. The two guard cavities are also differentially heated so that the same natural convection flow is established there. Under these conditions, the walls separating the cavities are planes of symmetry, which improves the insulation of these walls. Those three cavities are separated by 1 mm thick transparent polycarbonate walls ($\varepsilon \in [0.92; 0.96]$) to allow the visualization of the flow. The two guard cavities are insulated from the outside by an air gap.

The temperature of the isothermal walls is applied by a water circulation located on their outer face. The temperature of the circulation is controlled by means of two thermostatic baths (temperature stability : 0.02 K). To reach a Rayleigh number for this study equal to $Ra_H = (1.10 \pm 0.04) \times 10^8$ and for a mean temperature $T_0 = \frac{1}{2}(T_c + T_h)$ of 293 K, the temperature difference between the hot wall and the cold wall, $\Delta T = T_h - T_c$, is set at 9.50 K. In order to ensure the temperature uniformity of the duralumin walls, the temperature difference between the inlet and the outlet of these circulations is measured by thermocouples. This difference is found to be smaller than 0.10 K.

A particular attention was taken to ensure that the average temperature of the two thermostatic baths, T_0 , is close to the ambient temperature (measured by a Pt100 probe) in order to minimize heat exchanges between the cavity and the room. The temperature T_0 is set so that the difference between T_0 and the ambient temperature is smaller than 0.5 K.

2.2. Temperature measurements

The temperature is measured in the vertical mid-depth plane (located at $y = 7$ cm, i.e. $Y = 0.146$) by a K-type mobile micro-thermocouple (see Fig.

2 (left)). This micro-thermocouple, of $12.7 \mu\text{m}$ diameter, is compensated (at its cold junction) by another thermocouple located in an environment of high thermal stability (variation below 0.01 K during each temperature measurement) whose temperature is continuously recorded. In order to minimize the disturbance of the flow due to the temperature probe, the micro-thermocouple is inclined at 45° with respect to the vertical flow and placed at the end of a rigid rod with a diameter of 4 mm , located in a plane behind the measurement plane. The rod displacement within the median plane is provided by a motorized system implemented on two orthogonal axes. The top wall is extruded on a width of 6 mm to allow the rod access, and a sliding groove system is installed on the outer face of the top wall. The measurement uncertainty on the temperature is less than 0.2 K .

2.3. Heat transfer measurements

Heat transfer on the hot wall is quantified by the local Nusselt number, $Nu_{1D}(Z)$, which is equal to the dimensionless temperature gradient at the wall : $-\frac{\partial\theta}{\partial X}(Y = 0.146, Z)$. In order to measure this gradient, the micro-thermocouple is progressively moved away from the wall by $100 \mu\text{m}$ increments. The slope of the mean temperature profile over 5 measuring points gives the local measurement of the Nusselt number. This number of points enables to stay close to the wall in a linear temperature profile region while keeping a sufficient number of points to reduce the uncertainty on the calculated slope (correlation coefficient : $R^2 > 0.995$). This method leads to an uncertainty of less than 10% on the Nusselt number value.

2.4. Velocities measurements

Horizontal and vertical velocity components are measured in the mid-depth plane by PIV technique (see Fig. 2 (right)). The flow tracers are particles of paraffin oil ($\rho = 856 \text{ kg.m}^{-3}$) of a few micrometers diameter and provided by a smoke generator. The laser beam is created by a double-head Nd-YAG Litron laser. The laser beam, of 4 ns duration, emits a 1 mm thick laser sheet by means of optical lenses.

Particle observation is achieved by a *9.2 Phantom* CCD camera with a resolution of $1632 \times 1200 \text{ pixels}^2$. The pixel size is $11.5 \mu\text{m} \times 11.5 \mu\text{m}$ and their dynamic range is chosen at 12 bits. The scale factor, which is the ratio of the size of an object to the size of its image, is equal to 6.39. This scale factor results in an image with a spatial resolution of $12.0 \times 8.8 \text{ cm}^2$, so that the width of the image matches with the width of the cavity.

Each measurement contains 512 pairs of images recorded at the acquisition rate of 5 Hz . The duration between two images of a pair is 3 ms . The background is subtracted from each image to enhance the contrast. The low

flow speed in the center area of the cavity is determined with another pairs of images, constructed by taking the first image of two successive original pairs, which enables to determine the small corresponding displacements. For both processing techniques, image processing is carried out by using 64×64 initial and 32×32 final interrogation window size with a 50% overlap to enhance the velocity fields resolution. Velocity ranges covered by these two processings overlap.

2.5. Comparison with previous studies for an undisturbed flow

A comparison is made with previous studies on an undisturbed flow at $Ra_H = (0.92 \pm 0.03) \times 10^8$ to ensure both that this experimental device correctly reproduces a reference DHC flow and that the measurement methods are able to measure it accurately. For this purpose, profiles of temperature and vertical velocity component at mid-height, from $X = 0$ up to $X = 0.07$ are plotted in Fig. 3. The profiles are compared with the profiles obtained in an experimental study [25] at $Ra_H = 0.92 \times 10^8$ and with a 2D numerical simulation [26] at $Ra_H = 0.90 \times 10^8$. Concerning the temperature profiles, the maximum deviation with the experimental reference profile is equal to 0.016, lower than the maximal estimated uncertainties $(\delta\theta)_{max} = 0.027$. A larger difference (up to 0.034) is observed with the profile coming from the 2D numerical simulation. This difference remains however close to the estimated uncertainties. For the velocity profiles, the observed deviations compared to the profile from [25], all below 0.016, are lower or close to the measurement uncertainties $\delta W = 0.010$. The difference with the numerical results from [26] is related to the three-dimensional flow. The stratification parameter S , which is equal to the vertical temperature gradient at the center of the cavity, is compared to the value from [25] in Table 1. The measured stratification parameter fits with the reference one in regard of the uncertainties. Hence, a good agreement between our measurements and reference data is noticed which validate the measurement methods and ensure the quality of the undisturbed reference flow. The case without obstacle is now called *reference case*.

2.6. Cylindrical obstacle

A cylindrical obstacle (CO) is now introduced into the DHC and positioned in the median plane on the hot wall. This obstacle is a cylinder with a radius of 1 cm (dimensionless radius $r = 0.021$) and its axis is set orthogonal to the wall. In one case, the obstacle is thermally passive (very low conductivity) in order to only influence on its own the dynamic of the flow that rounds it. In that first case, it is called *insulating CO*. In the other case, the obstacle is thermally active (high conductivity) in order to additionally influence on

its own the temperature of the circumventing flow. In that second case it is called *conducting* obstacle.

The materials chosen for the insulating CO and the conducting CO are respectively cork and aluminum. Cork has a low thermal conductivity, which leads to a conductivity ratio against air equal to 1.8. On the contrary, aluminum conductivity ratio against air is higher than 9000. To ensure that the aluminum CO is actually close to the perfectly conducting case, the corresponding Biot number is calculated. For a CO of 2 cm length (dimensionless length $l = 0.042$) and an exchange coefficient h taken at $5 \text{ W.m}^{-2}.\text{K}^{-1}$, the Biot number is calculated as follows :

$$Bi = \frac{hV_{CO}}{\lambda S_{CO}} = \frac{h(\pi r^2 l)H}{\lambda(2\pi r l + \pi r^2)} = 8.5 \times 10^{-5}$$

where V_{CO} and S_{CO} are the volume and the surface of the obstacle, respectively. As $Bi \ll 1$, the thermal gradient within the conducting CO is negligible, and the conducting CO is almost isothermal. The insulating and the conducting CO are stuck on the hot wall with double-sided tape. This tape introduces a thermal resistance causing a temperature drop between the CO and the hot wall. In order to determine this temperature drop, the temperature on the tip of the conducting CO is measured by positioning the micro-thermocouple in contact with it. Indeed, as the conducting CO is isothermal, the temperature on its external face is equal to the temperature on the external side of the adhesive tape. A gap of 1 K is measured between the temperature of the conducting CO and the temperature of the hot wall. This gap represents only 10% of the temperature gap between isothermal walls ΔT . Finally, the adiabaticity of the insulating CO is checked with the measurement of the local Nusselt number at the center of its tip. For the 2 cm insulating CO, $Nu_{1D}(Z = Z_{CO}) = 1.4$ is found. Since $Nu_{1D}(Z = Z_{CO})$ is very low, there is negligible convective exchanges between the tip of the insulating CO and the fluid.

3. Results

3.1. Influence of the obstacle length

Three obstacle lengths are studied in this part. These lengths are equal to 0.5 cm, 1 cm and 2 cm, which corresponds to dimensionless lengths of $l = 0.010$, $l = 0.021$ and $l = 0.042$ respectively. They are chosen so that the obstacles are smaller or almost reach the size of the dynamic boundary layer (described in the next paragraph). The CO center is located at $Z_{CO} = 0.25$,

i.e. at the beginning of the boundary layer and outside the recirculation zone at the bottom of the cavity. This also enables to obtain a large zone downstream the CO on the hot wall. Throughout this study the Rayleigh number is set at $Ra_H = (1.10 \pm 0.04) \times 10^8$, which corresponds to the beginning of the unsteady laminar boundary layers flow regime [27] for the reference case configuration.

Vertical velocity component

The time-averaged fields of the vertical velocity component for the case without obstacle and the cases with insulating and conducting CO of lengths $l = 0.021$ and $l = 0.042$ are plotted in Fig. 4. The observation area ranges from $Z = 0.20$ (upstream and close to the CO) to $Z = 0.60$ (far downstream) across all the width of the DHC. The location of the CO, the streamlines as well as the dynamic boundary layer thickness, $\delta_{5\%}$, are also represented. $\delta_{5\%}$ corresponds to the abscissa for which the speed is equal to 5% of maximum or minimum speed (depending on which boundary layer is considered) :

$$\text{for a given } Z, \begin{cases} W(X = \delta_{5\%}(Z)) = 0.05 \max[W(X)] & \text{hot wall side} \\ W(X = \delta_{5\%}(Z)) = 0.05 \min[W(X)] & \text{cold wall side} \end{cases}$$

In the reference case, the boundary layers are vertical and their thickness is $\delta_{5\%} = 0.05 \pm 0.005$. The value of the uncertainty is taken as the size of an interrogation window of the PIV technique. Inside the hot boundary layer, the maximum velocity increases from $W_{max} = 0.18$ at $Z = 0.20$ to $W_{max} = 0.22$ at $Z = 0.60$. Even if a complex flow is observed in the stratified core, the velocity values are at least four orders of magnitude smaller than the velocity within the boundary layers. Therefore, this secondary flow does not take a significant part in the energy transport from the hot wall to the cold wall, this transport being carried out by the main flow along the walls. This is why the study focuses on this part of the flow.

The introduction of the insulating CO causes a deviation of a part of the flow around the tip of the CO (see Fig. 4, left). This deviation is quantified through the displacement of the location of $\delta_{5\%}$. With $l = 0.021$, $\delta_{5\%}$ reaches its maximum value 0.070 ± 0.005 at $Z = 0.30$, while for $l = 0.042$, $\delta_{5\%}$ exceeds 0.094 ± 0.005 around $Z = 0.27$. For those two lengths, the flow gradually rejoins a boundary layer thickness close to the one observed for the reference case. Moreover, there is, in the vertical mid-plane, a low velocity area directly downstream the CO, linked to the blocking effect of the obstacle.

For the conducting CO (Fig. 4, right), the deviation of the flow is less pronounced : $\delta_{5\%}$ reaches 0.057 ± 0.005 for $l = 0.021$ and 0.089 ± 0.005 for

$l = 0.042$. In addition, the thickness of the hot boundary layer approaches the value of the reference case farther than for the insulating obstacle case. In particular, $\delta_{5\%}$ is equal to 0.061 at $Z = 0.60$ for the conducting CO and $l = 0.042$, against 0.054 for the insulating one with the same length. However, the vertical velocity component within the boundary layer is larger with the conducting CO. For instance, for $l = 0.042$ the maximum vertical velocity is $W_{max}(Z = 0.60) = 0.27$ for the conducting CO, versus 0.23 for the insulating one. As for the insulating CO, a low velocity area is located directly downstream. However, the area is smaller for the conducting obstacle than for the insulating one. These differences are due to the development of a thermal plume downstream the conducting CO and will be analyzed further in more details in the thermal analysis part.

For the two lengths and the two types of obstacles considered, no change is observed for the vertical velocity or for the thickness of the boundary layer on the cold wall. Thus, the impact of the flow modification does not spread to the opposite wall. In addition, it can be noted that the secondary flow in the central zone is strongly disturbed by the presence of the obstacle. However, velocities in this area appear to be too small to influence significantly heat transfers, as shown thereafter.

In order to quantify the flow modification at the CO location, profiles of vertical velocity component, at $Z = 0.25$ for the insulating and the conducting CO and for the lengths $l = 0.010$, $l = 0.021$ and $l = 0.042$, are plotted in Fig. 5. This elevation ($Z = 0.25$) corresponds to the location of the CO center. The profiles on the cold side (Fig. 5, right) are plotted versus X . These profiles confirm that the flow modification does not reach the cold wall whatever the type of the OC (conducting or insulating).

The profiles on the hot side of the DHC are plotted (Fig. 5, left) versus relative abscissa, defined as $X_{rel} = X - l$, in order to compare the flow from the tip of the obstacle whatever its length. The profiles in absolute abscissa X are also inserted in this figure.

For the insulating and the conducting CO with the smallest length, $l = 0.010$, profiles on the hot side in relative abscissa are close to the profile obtained without obstacle. As no drop of velocity is observed in these cases, nearly all the flow seems to be deviated on the tip of the CO. For $l = 0.021$, a reduction of the maximum of velocity is observed. The amount of flow that is deviated along the tip of the CO has also decreased, which means that a part of the flow circumvents the obstacle by front and back sides. This effect is amplified for the longest obstacle, $l = 0.042$.

On the right part of these profiles for the conducting case, the vertical velocity component tends to reach the near zero value of the stratified core at a lower abscissa than for the insulating ones. This behavior is related to

an increase of the temperature difference and consequently of the buoyancy forces in front of the conducting CO, being isothermal at a temperature close to the hot wall temperature. This assert will be verified by measuring the temperature of this deviated flow.

Deviated flow temperature

Temperature profiles from the tip of the insulating and conducting CO for the three lengths studied and the reference case are plotted in Fig. 6, at $Z = 0.25$, corresponding to the vertical location of the center of the obstacle. There are plotted against the relative abscissa, X_{rel} , which enables to describe, in terms of temperature, the deviated flow shown in Fig. 5.

For the insulating obstacle, a temperature drop is observed at the tip of the CO ($X_{rel} = 0$) when compared to the case without obstacle. This temperature drop is larger for longer obstacles : for lengths $l = 0.010$, $l = 0.021$ and $l = 0.042$, the temperature at the tip ($\theta(X_{rel} = 0)$) are equal to 0.22, 0.11 and -0.04 respectively, which must be compared to a value close to $\theta_h = 0.50$ in the reference case. The temperature of the deviated flow is then lower than the temperature of the flow measured in front of the hot wall, without obstacle, at the same vertical elevation. Indeed, the flow coming from the upstream hot boundary layer does not exchange heat with the adiabatic CO and reaches an area that is located partially or totally in the stratified core. Furthermore, for the considered elevation $Z = 0.25$, the temperature of the stratified core is equal to $\theta = -0.15$. As the deviated flow reaches a colder environment, a heat exchange occurs which decreases the temperature of the deviated flow. For all the profiles, the temperatures progressively reach the stratification temperature when X_{rel} increases. Note that, the stratification temperature is determined when the profile reaches the core temperature at a given elevation.

For the conducting obstacle, the temperature of the deviated flow is close to the temperature inside the hot boundary layer without obstacle at the same relative location. Only a small temperature decrease is noticed at the tip of the conducting CO. Hence, as the conducting CO is quasi-isothermal with a temperature close to the one of the hot wall, the temperature profiles on the external side of the obstacles are the same as along the hot wall, regardless the length of the obstacle. The deviated flow maintains its upstream temperature although it reaches the stratified core at a colder temperature. Finally, as for the insulating case, temperatures reach progressively the stratification temperature when X_{rel} increases.

As the deviated flow returns to the vicinity of the hot wall, downstream the CO, these observed changes on the temperature and the structure of the flow will influence the downstream heat transfers.

Downstream heat transfers

Local Nusselt numbers $Nu_{1D}(Z)$ have been measured along the hot wall downstream the CO, for lengths $l = 0.021$, $l = 0.042$ and for the reference case (see Fig. 7). $Nu_{1D}(Z)$ is the local Nusselt number in the vertical mid-depth plane ($Y = 0.146$) at the elevation Z . The measurement area in the vertical mid-depth plane starts at $Z = 0.30$, directly downstream the CO, and goes up to $Z = 0.80$, in steps of 0.10. Beyond $Z = 0.80$ no changes are observed on heat transfer.

For the insulating obstacle, an increase of local Nusselt numbers, compared to the reference case, is noticed close to the CO. This increase is more important for the longest CO ($l = 0.042$) than for the other ($l = 0.021$). As Z increases, Nusselt numbers tend to the value of the reference case. Beyond $Z = 0.50$ and considering the measurement uncertainties, they are similar to those obtained in the reference case. The insulating CO has thus locally increased heat transfer downstream the obstacle. This can be attributed to the temperature decrease of the deviated flow observed in Fig. 6 : when this flow returns to the vicinity of the hot wall, its temperature is lower than the temperature of the hot boundary layer in the reference case. This leads to a heat transfer increase due to a larger difference between the flow temperature and the wall temperature. In addition, the deviated backflow induces an impacting jet on the wall, which also increases heat transfer compared to a boundary layer flow parallel to the wall.

For the conducting obstacle, an opposite effect is observed : the heat transfer decreases downstream the CO compared to the reference case. The longest CO leads to the largest changes on Nusselt numbers. As for the insulating CO, the local Nusselt numbers progressively reaches the value of the reference case when moving downstream. However, for the conducting case, the location of the convergence is farther at $Z = 0.70$. $Nu_{1D}(Z)$ is smaller for $l = 0.042$ than for $l = 0.021$ up to the convergence location at $Z = 0.70$. The decrease observed on downstream heat transfer, for the conducting case, is due to the heating of the flow by the conducting CO : as this CO is isothermal ($T_{CO} \approx T_h$), the flow that circumvents the CO is heated. The flow temperature increases in the boundary layer, downstream the CO. It results in a reduction of the temperature difference with the wall, and consequently in a smaller heat transfer. Moreover, $Nu_{1D}(Z = 0.30)$ are close for the two considered lengths and much lower than the value of the reference case. Indeed, at this location, Fig. 4 showed that the velocity is lower here due to a blocking effect of the obstacle. The similar heat transfers in this area are probably due to close velocities and temperatures for both

cases.

In order to quantify the heat transfer modifications in the downstream area, the local Nusselt numbers are integrated over $Z \in [0.30; 0.80]$. The integrated Nusselt numbers downstream the CO, $Nu_{1D,d}$, are calculated as follows :

$$\begin{aligned} Nu_{1D,d} &= \frac{1}{Z_2 - Z_1} \int_{Z_1=0.30}^{Z_2=0.80} Nu_{1D}(Z) dZ \\ &= \frac{1}{Z_2 - Z_1} \frac{0.10}{2} \left(\sum_{Z_i=0.40}^{0.70} Nu_{1D}(Z_i) + \sum_{Z_i=0.30}^{0.80} Nu_{1D}(Z_i) \right) \end{aligned}$$

To compare these integrated Nusselt numbers with the one in the reference case, the relative gain on downstream heat transfer G_{Nu} is defined as :

$$G_{Nu} = \frac{Nu_{1D,d} - (Nu_{1D,d})_{ref}}{(Nu_{1D,d})_{ref}}$$

The downstream Nusselt numbers and the relative gains are given in Table 2. In the reference case, the integrated Nusselt number is equal to 5.88 ± 0.26 .

For the insulating obstacle, $Nu_{1D,d}$ is higher and exceed 3. The increase for the longest insulating CO compared to the reference case is equal to 6 %, only slightly larger than the increase of 4 % for the CO of length $l = 0.021$.

On the contrary, integrated Nusselt numbers for the conducting obstacle are reduced compared to the reference case : for the lengths $l = 0.021$ and $l = 0.042$ decreases are respectively about -9% and -15% . In absolute value and for each size, the relative changes for the conducting CO are larger than for the insulating ones.

The relative gains observed for insulating and conducting obstacles are due to different effects induced by each type of CO :

- For the insulating CO, it has been shown that the heat transfer reduction is linked to the deviation of a part of the flow, which reaches the stratified area and gets colder before returning to the vicinity of the hot wall. This heat transfer modification is only due to an obstacle effect : by acting on the flow, the downstream heat transfer is modified.
- For the conducting CO, there is also an obstacle effect, indeed the obstacle is set at the same location and has the same size (the streamlines are also deviated, see Fig. 4, right). However, the CO temperature is close to the hot wall temperature, generating a hot thermal plume.

Hence, a competition occurs between the obstacle effect which leads to an increase of downstream heat transfer (as for insulating CO) and a thermal effect which reduces heat transfer by heating the flow. In that case, the thermal effect is stronger than the obstacle one.

The influence of obstacle length has been described in terms of flow modification, thermal effect and downstream heat transfer changes. These results have been found for an obstacle located at $Z_{CO} = 0.25$. In order to determine if these results are similar for other obstacle locations, the influence of the obstacle vertical location on heat transfers is studied.

3.2. Influence of the obstacle vertical location

As the relative change on heat transfer is increasing with the CO length, the highest value ($l = 0.042$) is now chosen. This length allows to observe larger effects on heat transfer. Several elevations of the obstacle, Z_{CO} , have been studied along the vertical mid-depth plane on the hot wall side. In addition to the previous location ($Z_{CO} = 0.25$) the insulating and conducting obstacles are successively placed from $Z_{CO} = 0.35$ to $Z_{CO} = 0.65$ by step of 0.10. Local Nusselt numbers are measured upstream and downstream the CO, from $Z = 0.10$ to $Z = 0.90$ and are presented in Fig. 8. The bottom and the top of the obstacle are represented with dashed-lines. Integrations of $Nu_{1D}(Z)$ over the upstream and the downstream parts, $Nu_{1D,u}$ and $Nu_{1D,d}$, are defined as :

$$Nu_{1D,u} = \frac{1}{(Z_{CO}-0.05)-0.10} \int_{0.10}^{Z_{CO}-0.05} Nu_{1D}(Z) dZ$$

$$Nu_{1D,d} = \frac{1}{0.90-(Z_{CO}+0.05)} \int_{Z_{CO}+0.05}^{0.90} Nu_{1D}(Z) dZ$$

Note that for the reference case, the same integration area is considered even if no obstacle exists for that case. For all the obstacle locations, almost no changes on upstream heat transfer are observed. The differences noticed are probably only due to measurement uncertainties.

For the insulating CO, an increase of downstream heat transfers is observed, compared to the reference case, for all the obstacle locations. For $Z_{CO} = 0.25$, on the first location beyond the CO, $Nu_{1D}(Z)$ has increased from 9, in the reference case, to around 11, in the insulating CO case. Whereas, for $Z_{CO} = 0.65$, on the first location beyond the CO, $Nu_{1D}(Z)$ has increased from 4 to around 10. Thus, the relative increase is more pronounced for high locations of the obstacle.

For the conducting CO, the relative change compared to the reference case depends on the obstacle location. For $Z_{CO} = 0.25$ and $Z_{CO} = 0.35$, a decrease of the downstream heat transfer is noticed. For $Z_{CO} = 0.45$ and $Z_{CO} = 0.55$, $Nu_{1D}(Z)$ for conducting CO is very close to the reference case. For $Z_{CO} = 0.65$, a significant increase of the downstream heat transfer is observed. Hence, for a higher obstacle location, the conducting CO leads progressively from a heat transfer reduction to a heat transfer increase when compared to the reference case. As for the insulating CO, this modification is not connected to an increase of $Nu_{1D}(Z)$ downstream the CO for higher value of Z : $Nu_{1D}(Z)$ remains quite similar to the first location downstream the obstacle, but the associated Nusselt number for the reference case decreases for higher location.

As previously noticed, for all the values of Z_{CO} , integrated Nusselt numbers upstream the obstacle, $Nu_{1D,u}$, are similar for the reference case and for cases with obstacle. To quantify integrated Nusselt numbers downstream the obstacle, relative gains G_{Nu} are given in Table 3 for each obstacle elevation and for insulating and conducting CO.

For both obstacle conductivities, G_{Nu} progressively increases. For the insulating CO, gains are positive and vary from +8% for $Z_{CO} = 0.25$ to +83% for $Z_{CO} = 0.65$. For the conducting CO, G_{Nu} is first negative : -19% for $Z_{CO} = 0.25$, then close to zero for $Z_{CO} = 0.45$ and positive, up to +25% for the highest location $Z_{CO} = 0.65$. This is consistent with the previous analyses.

4. Conclusions and perspectives

A natural convection flow in a differentially heated cavity of aspect ratio 4 was disturbed by means of a localized cylindrical obstacle. The obstacle was placed on the hot wall in the mid-depth plane of the cavity.

Two kinds of obstacles are considered : an insulating obstacle that only influences on its own the dynamics of the flow that rounds it and a conductive obstacle that influences on its own both the dynamics and the temperature of the flow that rounds it.

The effects, in the mid-depth plane, of the obstacle length and location were studied through the analysis of velocity fields, thermal profiles and heat transfers. The following conclusions can be drawn :

- Firstly, the obstacle is placed at the beginning of the hot boundary layer :
- for the insulating obstacle, the upstream flow is deviated toward the core of the cavity. This part of the cavity is colder, which decreases the temperature of the flow. Consequently, when it returns to the vicinity

of the hot wall, the heat transfer downstream the obstacle increases when compared to the reference case (without obstacle).

- for the conducting obstacle, the flow is also deviated toward the core of the cavity. However, the heat exchange with the obstacle maintains the temperature of the deviated flow. Furthermore, the flow that rounds the obstacle by the front and back sides is heated, inducing a thermal plume. This results in a decrease of the heat transfer downstream the obstacle.
- For both insulating and conducting obstacles, these effects are enhanced for longer obstacles.

Secondly, the influence of the vertical location of the obstacle on the hot wall is analyzed :

- for both insulating and conducting obstacles, no influence is noticed upstream the obstacle.
- for both insulating and conducting obstacles, the relative gain on heat transfer downstream the obstacle, compared to the case without obstacle, increases with the vertical location. For the insulating obstacle, the relative gain starts at +8 % for an obstacle located at $Z = 0.25$ and reaches +83 % for an obstacle located at $Z = 0.65$. For the conducting obstacle the relative gain is negative and equal to -19 % for an obstacle located at $Z = 0.25$ and reaches +25 % for an obstacle located at $Z = 0.65$. This increase of the relative gain is due to the decrease of the heat transfer with the vertical position in the reference case whereas, for both conductivities, heat transfer downstream the obstacle remains almost constant whatever the vertical location.

Several perspectives to this work can be given :

- Firstly, from the experimental point of view, an analysis of the influence of several obstacles could be interesting.
- Secondly, as the data provided in this paper can be used for numerical code validation, such an approach would allow to investigate the influence of the obstacles into the whole cavity.

5. Acknowledgments

The authors would thank CPER (2015-2020) and ERDF (2014-2020) grants for supporting this work through the funding of experimental equipment. The authors would also like to thank H. Arlaud who built the micro-thermocouples and the experimental set-up, C. Fuentes for her help with laser techniques and C. Calbrix for his help for the measurements.

Références

- [1] G. D. Davis, Natural-convection of air in a square cavity - a bench-mark numerical-solution, *International Journal Numerical Methods Fluids* 3 (1983) 249–264.
- [2] N. C. Markatos, K. A. Pericleous, Laminar and turbulent natural convection in an enclosed cavity, *International Journal of Heat and Mass Transfer* 27 (1984) 755–772.
- [3] S. Xin, P. Le Quéré, Direct numerical simulations of two-dimensional chaotic natural convection in a differentially heated cavity of aspect ratio 4, *Journal of Fluid Mechanics* 304 (1995) 87–118.
- [4] F. X. Trias, M. Soria, A. Oliva, C. D. Perez-Segarra, Direct numerical simulations of two- and three-dimensional turbulent natural convection flows in a differentially heated cavity of aspect ratio 4, *Journal of Fluid Mechanics* 586 (2007) 259–293.
- [5] D. Saury, N. Rouger, F. Djanna, F. Penot, Natural convection in an air-filled cavity : Experimental results at large rayleigh numbers, *International Communications In Heat and Mass Transfer* 38 (2011) 679–687.
- [6] V. Kishor, S. Singh, A. Srivastava, Investigation of convective heat transfer phenomena in differentially-heated vertical closed cavity : Whole field experiments and numerical simulations, *Experimental Thermal and Fluid Science* 99 (2018) 71–84.
- [7] Y. Lin, B. Farouk, Heat transfer in a rectangular chamber with differentially heated horizontal walls : Effects of a vibrating sidewall, *International Journal of Heat and Mass Transfer* 51 (2008) 3179–3189.
- [8] S. Hyun, D.-R. Lee, B.-G. Loh, Investigation of convective heat transfer augmentation using acoustic streaming generated by ultrasonic vibrations, *International Journal of Heat and Mass Transfer* 48 (2005) 703–718.
- [9] F. Penot, O. Skurtys, D. Saury, Preliminary experiments on the control of natural convection in differentially-heated cavities, *International Journal of Thermal Sciences* 49 (2010) 1911–1919.
- [10] P. Chorin, F. Moreau, D. Saury, Heat transfer modification induced by a localized thermal disturbance in a differentially-heated cavity, *International Journal of Thermal Sciences* 125 (2018) 101–110.

- [11] D. Saury, A. Benkhelifa, F. Penot, Experimental determination of first bifurcations to unsteady natural convection in a differentially-heated cavity tilted from 0 degrees to 180 degrees, *Experimental Thermal and Fluid Science* 38 (2012) 74–84.
- [12] Y. Du, P. Tong, Enhanced heat transport in turbulent convection over a rough surface, *Physical Review Letters* 81 (1998) 987–990.
- [13] J. Salort, O. Liot, E. Rusaouen, F. Seychelles, J.-C. Tisserand, M. Creysseles, B. Castaing, F. Chilla, Thermal boundary layer near roughnesses in turbulent rayleigh-benard convection : Flow structure and multistability, *Physics of Fluids* 26 (2014).
- [14] M. Yousaf, S. Usman, Natural convection heat transfer in a square cavity with sinusoidal roughness elements, *International Journal of Heat and Mass Transfer* 90 (2015) 180–190.
- [15] S. Shakerin, M. Bohn, R. Loehrke, Natural convection in an enclosure with discrete roughness elements on a vertical heated wall, *International Journal of Heat and Mass Transfer* 31 (1988) 1423–1430.
- [16] A. Nag, A. Sarkar, V. Sastri, Natural-convection in a differentially heated square cavity with a horizontal partition plate on the hot-wall, *Computer Methods in Applied Mechanics and Engineering* 110 (1993) 143–156.
- [17] G. Polidori, J. Padet, Transient free convection flow on a vertical surface with an array of large-scale roughness elements, *Experimental Thermal and Fluid Science* 27 (2003) 251–260.
- [18] S. H. Tasnim, M. R. Collins, Numerical analysis of heat transfer in a square cavity with a baffle on the hot wall, *International Communications in Heat and Mass Transfer* 31 (2004) 639–650.
- [19] F. Xu, J. C. Patterson, C. Lei, Transition to a periodic flow induced by a thin fin on the sidewall of a differentially heated cavity, *International Journal of Heat and Mass Transfer* 52 (2009) 620–628.
- [20] F. Xu, J. C. Patterson, C. Lei, Unsteady flow and heat transfer adjacent to the sidewall wall of a differentially heated cavity with a conducting and an adiabatic fin, *International Journal of Heat and Fluid Flow* 32 (2011) 680–687.

- [21] F. Xu, Unsteady coupled thermal boundary layers induced by a fin on the partition of a differentially heated cavity, *International Communications in Heat and Mass Transfer* 67 (2015) 59–65.
- [22] M. Ghalambaz, E. Jamesahar, M. A. Ismael, A. J. Chamkha, Fluid-structure interaction study of natural convection heat transfer over a flexible oscillating fin in a square cavity, *International Journal of Thermal Sciences* 111 (2017) 256–273.
- [23] A. A. Merrikh, J. L. Lage, Natural convection in an enclosure with disconnected and conducting solid blocks, *International Journal of Heat and Mass Transfer* 48 (2005) 1361–1372.
- [24] O. Laguerre, S. Benamara, D. Remy, D. Flick, Experimental and numerical study of heat and moisture transfers by natural convection in a cavity filled with solid obstacles, *International Journal of Heat and Mass Transfer* 52 (2009) 5691–5700.
- [25] O. Skurtys, Contribution au contrôle de la convection naturelle par excitation thermique des couches limites en cavité différentiellement chauffée, Ph.D. thesis, Université de Poitiers, 2004.
- [26] E. Gadoin, P. Le Quéré, O. Daube, A general methodology for investigating flow instabilities in complex geometries : application to natural convection in enclosures, *International Journal for Numerical Methods in Fluids* 37 (2001) 175–208.
- [27] S. Xin, P. Le Quéré, Natural-convection flows in air-filled, differentially heated cavities with adiabatic horizontal walls, *Numerical Heat Transfer, Part A* 50 (2006) 437–466.

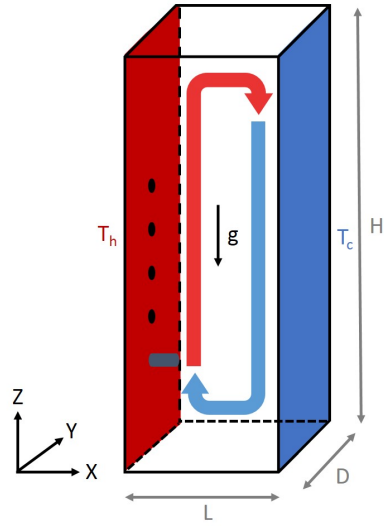


FIGURE 1: Scheme of the differentially heated cavity with a cylindrical obstacle located at $Z = 0.25$; other obstacle locations are drawn by black circles.

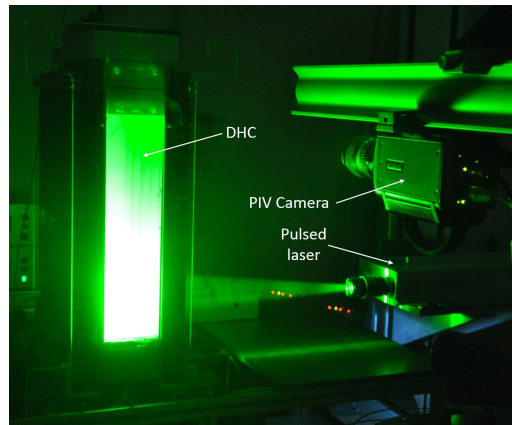
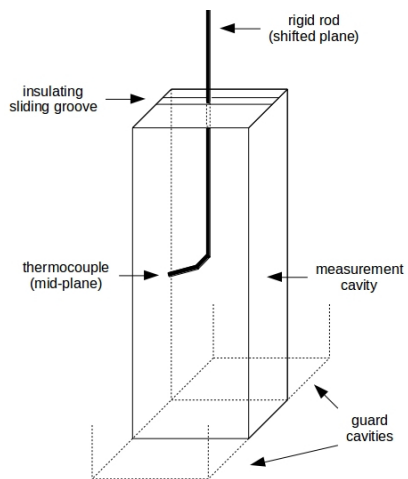


FIGURE 2: Scheme of the differentially heated cavities and temperature measurement set-up (left); experimental set-up for PIV measurements (right).

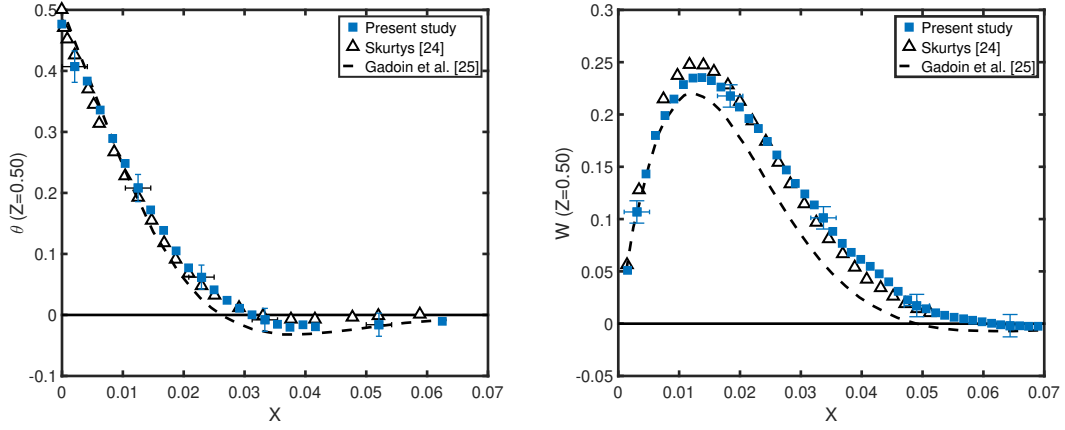


FIGURE 3: Temperature, θ , and vertical velocity component, W , along the X axis at $Z = 0.50$ and $Ra_H = (0.92 \pm 0.03) \times 10^8$; comparison with experimental data from [25] at $Ra_H = 0.92 \times 10^8$ and numerical data (2D simulations) from [26] at $Ra_H = 0.90 \times 10^8$.

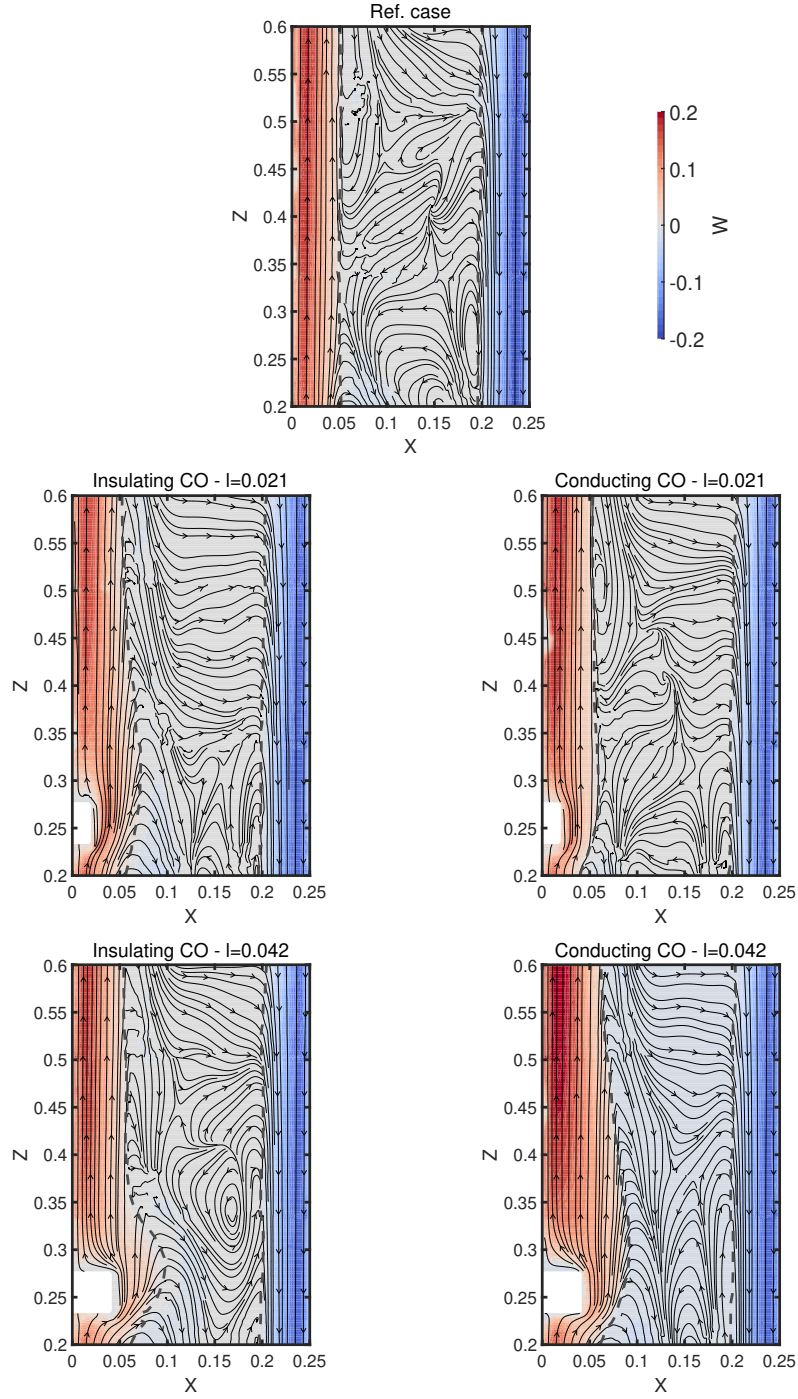


FIGURE 4: Fields of vertical velocity component, W , for several sizes ($l = 0$ (top), $l = 0.021$ (middle), $l = 0.042$ (bottom)) of insulating (left) and conducting (right) obstacles; streamlines and dynamic boundary layer thickness $\delta_{5\%}$ are overprinted.

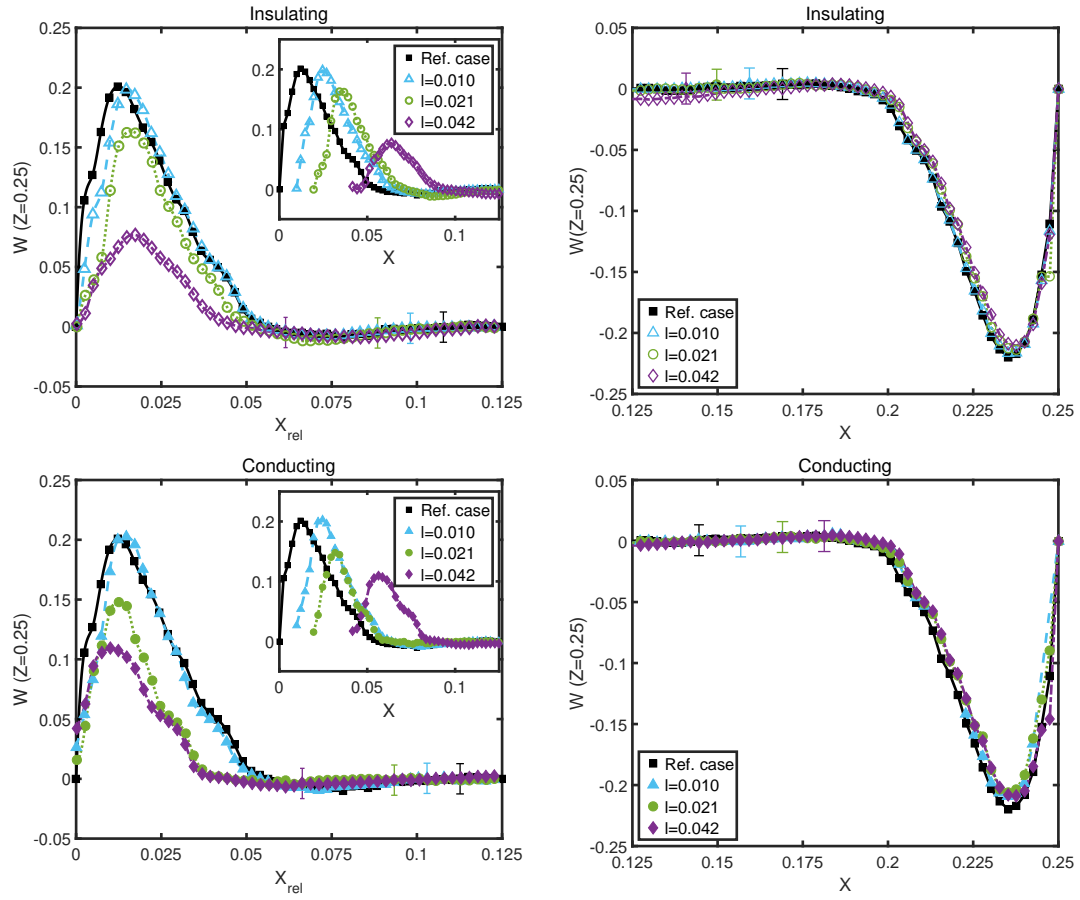


FIGURE 5: Profiles of vertical velocity component, W , along the $X_{rel} = X - l$ axis in the hot side mid-width (left) and along the X axis in the cold side mid-width (right), at $Z = 0.25$ for insulating and conducting cylindrical obstacles. Inset in (left) : profiles along the X axis.

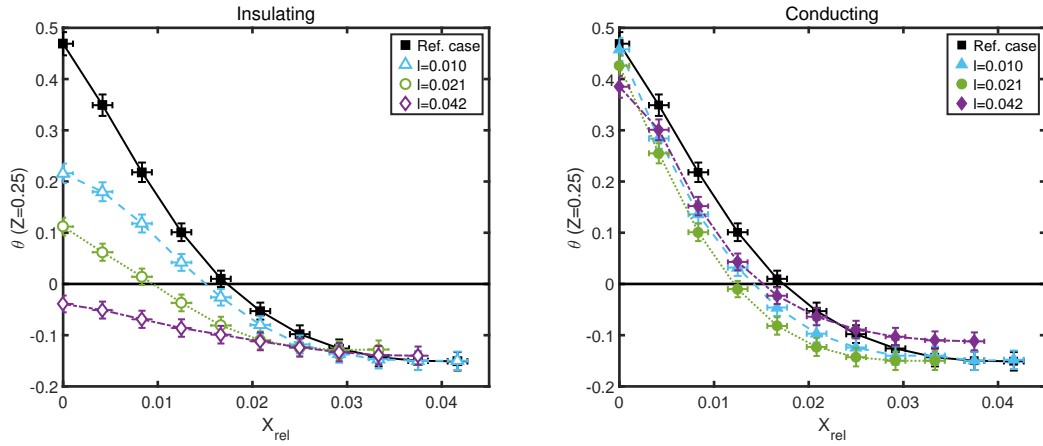


FIGURE 6: Temperature θ profiles at $Z = 0.25$ for insulating and conducting cylindrical obstacles.

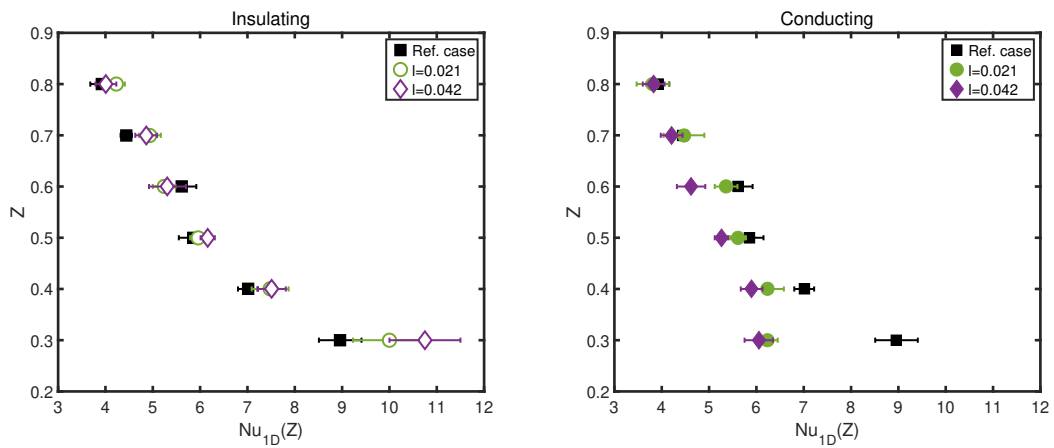


FIGURE 7: Local Nusselt numbers, $Nu_{1D}(Z)$, for $Z \in [0.30; 0.80]$ for insulating and conducting cylindrical obstacles.

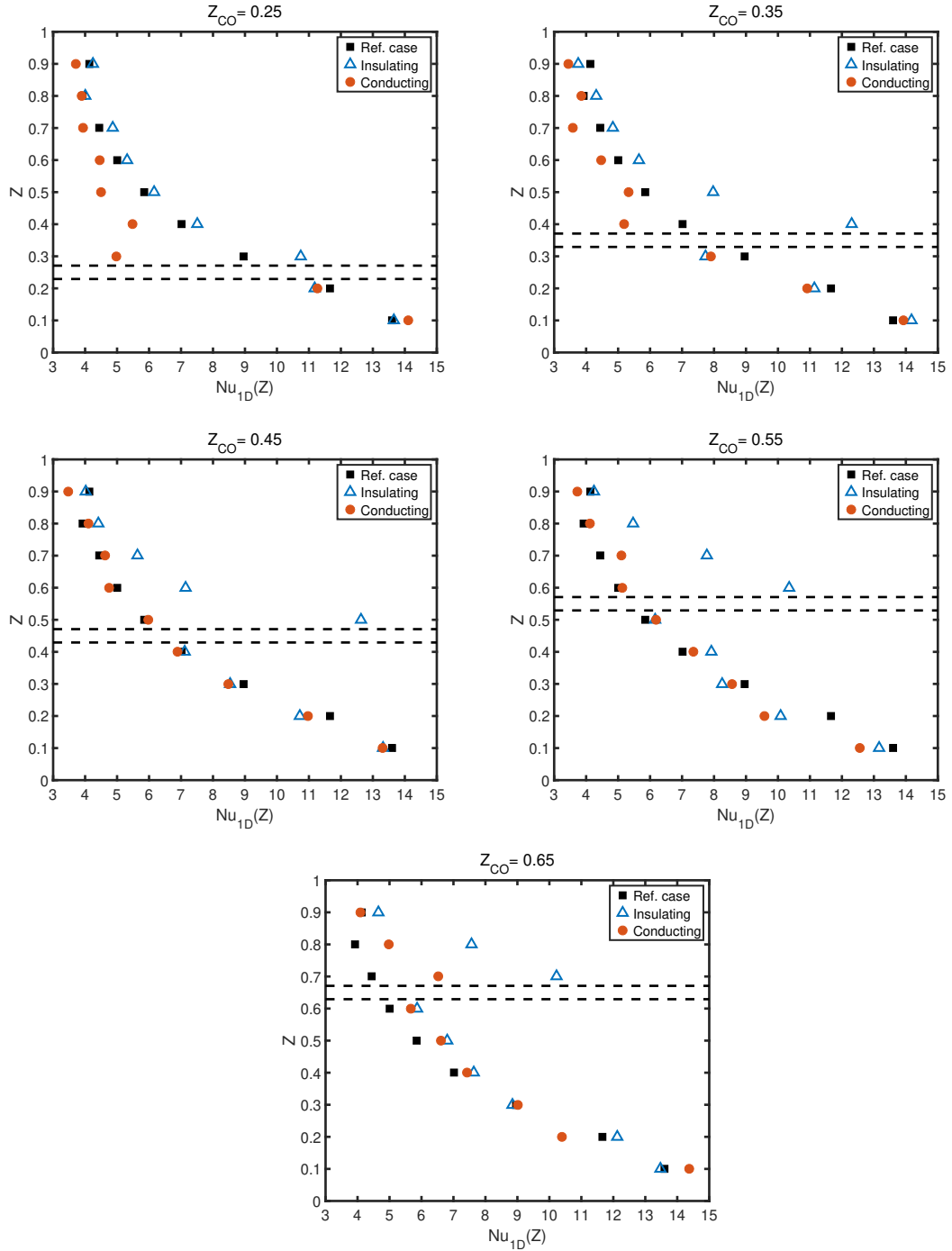


FIGURE 8: Local Nusselt numbers, $Nu_{1D}(Z)$, for several vertical locations, Z_{CO} , of the insulating and conducting cylindrical obstacles.

	Present Study	Skurtys [25]
S	0.54 ± 0.02	0.51 ± 0.02

TABLE 1: Stratification parameter S at $Ra_H = (0.92 \pm 0.03) \times 10^8$; comparison with [25].

	l	0	0.021	0.042
Insulating obstacles	$Nu_{1D,d}$	5.88 ± 0.26	6.14 ± 0.30	6.24 ± 0.32
	G_{Nu}	—	+4%	+6%
Conducting obstacles	$Nu_{1D,d}$	5.88 ± 0.26	5.34 ± 0.30	4.98 ± 0.24
	G_{Nu}	—	-9%	-15%

TABLE 2: Integration of local Nusselt numbers, $Nu_{1D,d}$, and gain relative to reference case, G_{Nu} , for reference case ($l = 0$) and insulating and conducting obstacles ($l = 0.021$ and $l = 0.042$).

	Z_{CO}	0.25	0.35	0.45	0.55	0.65
G_{Nu}	Insulating	+8%	+24%	+39%	+59%	+83%
	Conducting	-19%	-13%	-1%	+5%	+25%

TABLE 3: Gain relative to reference case, G_{Nu} , in the downstream part (from $Z_{CO} + 0.05$ to $Z = 0.90$), for each obstacle location, Z_{CO} , for insulating and conducting obstacles.